



POLİTEKNİK DERGİSİ

JOURNAL of POLYTECHNIC

ISSN: 1302-0900 (PRINT), ISSN: 2147-9429 (ONLINE)

URL: <http://dergipark.org.tr/politeknik>



Effects of the shaft speed on stiffness and damping coefficients of hydrodynamic bearing-shaft system under variable viscosity

Değişken viskozite altında şaft hızının hidrodinamik yatak-şaft sisteminin rijitlik ve sönüm katsayıları üzerindeki etkileri

Yazar(lar) (Author(s)): Abdurrahim DAL¹

ORCID¹: 0000-0002-7012-2148

To cite to this article: Dal A., “Effects of the Shaft Speed on Stiffness and Damping Coefficients of Hydrodynamic Bearing-Shaft System under Variable Viscosity”, *Journal of Polytechnic*, 28(1): 13-25, (2025).

Bu makaleye şu şekilde atıfta bulunabilirsiniz: Dal A., “Effects of the Shaft Speed on Stiffness and Damping Coefficients of Hydrodynamic Bearing-Shaft System under Variable Viscosity”, *Politeknik Dergisi*, 28(1): 13-25, (2025).

Erişim linki (To link to this article): <http://dergipark.org.tr/politeknik/archive>

DOI: 10.2339/politeknik.1424395

Effects of the Shaft Speed on Stiffness and Damping Coefficients of Hydrodynamic Bearing-Shaft System under Variable Viscosity

Highlights

- ❖ The Dowson's equation is derived for variable viscosity.
- ❖ The temperature distribution of the lubricant is modelled with 3-dimensional energy equation.
- ❖ Perturbation equation is derived for variable viscosity.

Graphical Abstract

The effects of the shaft speed on the stiffness and the damping coefficients, as well as the stability of the bearing-shaft system are investigated for variable viscosity dependent on the heat generation in the lubricant.

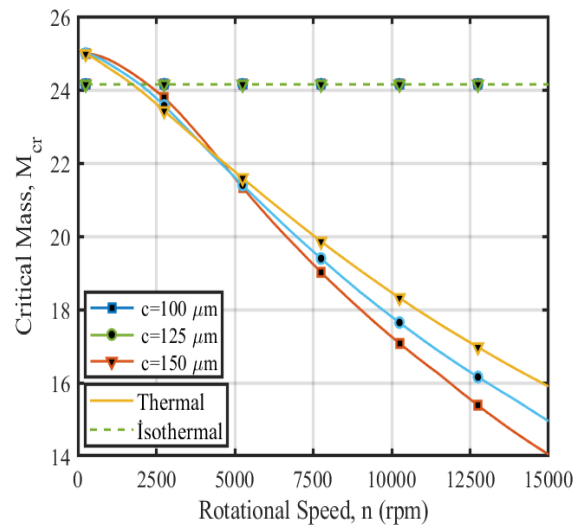


Figure. Critical mass of the system vs rotational speed

Aim

This study aims to investigate the effects of the shaft speed on the stiffness and the damping coefficients, as well as the stability of the bearing-shaft system for variable viscosity dependent on the temperature.

Design & Methodology

Lubricant flow is modelled with Dowson's equation, the temperature distribution is derived with 3-dimensional energy equation, and the pressure functions are derived from the perturbation equations for the dynamic coefficients. These mathematical models are solved with a developed algorithm.

Originality

The novelty of this study is an investigation of the effects of the shaft speed on the dynamic characteristics and stability of a hydrodynamic bearing-shaft system under variable viscosity dependent on the heat generation in lubricant.

Findings

It was determined that the high speed operations increase the lubricant temperature, and so the static and dynamic characteristics decrease, moreover, this effect is more dominant for the smaller radial clearance.

Conclusion

Although, the system operates in a stable region when the thermal effects are neglected, however, instability will cause trouble in the same speed due to rising temperatures.

Declaration of Ethical Standards

The author(s) of this article declare that the materials and methods used in this study do not require ethical committee permission and/or legal-special permission.

Effects of the Shaft Speed on Stiffness and Damping Coefficients of Hydrodynamic Bearing-Shaft System under Variable Viscosity

Research Article / Araştırma Makalesi

Abdurrahim DAL^{1*}

¹Engineering Faculty, Mechanical Engineering Department, Adana Alparslan Türkeş Science and Technology University, Adana, Türkiye

(Geliş/Received : 23.01.2024 ; Kabul/Accepted : 15.04.2024 ; Erken Görünüm/Early View : 28.04.2024)

ABSTRACT

The rotating shaft-hydrodynamic bearings systems operated with high speed and/or heavy load conditions expose serious rotor-dynamics instability problems due to characteristics of the supporting bearings. The stability and the dynamics of these systems, directly relate to the lubricant properties that are directly affect by the heat generation. The main purpose of this study is investigation of the dynamic characteristics and the stability of a shaft supported by hydrodynamic journal bearing under variable viscosity. The equations of lubricant flow were derived by Dowson's model under variable viscosity, and the dynamic characteristics were modelled with the perturbation model in direct and cross directions. The heat transfers between oil and the journal surface was modelled in a 3-dimensional energy and the heat conduction equation. An algorithm based on finite difference and successive-over-relaxation method was developed to solve the theoretical models, simultaneously, and a serial simulation was performed to investigate the variations of the dynamic coefficients of the bearing-shaft system concerning the shaft speed for different radial clearance values. It was determined that the high speed increases the lubricant temperature, and so the static and dynamic performance characteristics decrease, moreover, this effect is more dominant for the smaller radial clearance.

Keywords: Variable viscosity, dynamic characteristics, rotor dynamic, hydrodynamic bearing.

Değişken Viskozite Altında Şaft Hızının Hidrodinamik Yatak-Şaft Sisteminin Rijitlik ve Sönüm Katsayıları Üzerindeki Etkileri

ÖZ

Ağır yükler ve yüksek hızlarda çalışan hidrodinamik yatak-şaft sistemleri yatakların karakteristik özellikleri sebebiyle önemli rotor dinamiği kararsızlık problemlerine maruz kalırlar. Bu yatakların dinamik özellikleri ve kararlılıkları çalışma esnasında ortaya çıkan ısıdan doğrudan etkilenir. Bu makalede bir hidrodinamik yatak-şaft sistemi kararlılığının ve dinamik karakteristiklerinin değişken viskozite altında araştırılması amaçlanmaktadır. Yağlayıcının akışı değişken viskozite için Dowson denkleminde türetilmiş ve iki serbestlik dereceli bir yatak-şaft sistemi için pertürbasyon denklemleri elde edilmiştir. Yağ filmindeki ısı transferi 3-boyutlu enerji denklemi ile modellenmiş ve bu modele, yatak çapı yönünde meydana gelen ısı transferi de ısı iletim denklemi ile modellenerek dahil edilmiştir. Teorik modellerin eş zamanlı çözümü için, sonlu farklar metodunu esas alan bir çözüm algoritması geliştirilmiş ve şaft hızının farklı radial boşluğa sahip hidrodinamik yatakların dinamik katsayıları üzerindeki etkilerinin araştırılması için bir dizi benzetim gerçekleştirilmiştir. Yapılan benzetim sonuçları, şaft hızının artması ile yağ sıcaklığının arttığını ve yatağın statik ve dinamik özelliklerini azalttığı ve termal etkinin daha küçük boşluk değerleri için daha etkili olduğu tespit edilmiştir.

Anahtar Kelimeler: Değişken viskozite, dinamik karakteristikler, rotor dinamiği, radial hidrodinamik yatak.

1. INTRODUCTION

In rotating machinery such as turbine, compressors, pumps, etc., the hydrodynamic bearing is generally preferred to support a shaft through providing some important advantages. The oil which plays a vital role in the rotating machines, flows between journal and shaft surfaces, and it prevents the surface contact. Compared with gas and water-lubricated bearings, the oil-lubricated bearings can support heavier loads owing to high viscosity [1-2]. In these, as the thin lubrication film is in direct contact with the surfaces, dynamic characteristics, as well as stability of the rotating machinery strongly

relate to the physical properties of the lubricant. In industry, syntactically mineral oil based on paraffin is generally preferred as a lubricant, and the physical properties of these oils are dramatically affected by the temperature. Although the hydrodynamic bearings promise important advantages in the rotating machinery, they encounter some instability problems that are triggered by the temperature rising when operating under heavy load and/or high speed. As a result of these extreme operating conditions, the rise in the lubricant temperature due to the increasing friction between lubricant layers, causes decay of the viscosity. Therefore,

*Sorumlu Yazar (Corresponding Author)
e-posta : adal@atu.edu.tr

dynamic characteristics and the stability of the system affects by temperature rising in hydrodynamic journal bearings. Consequentially, it is important to analyze the stability and the characteristic of the high rotating speed bearing-shaft system considering variable viscosity, in other words, the thermal effects [3-6, 30-32].

In the past several decades, a lot of the investigations on the fluid-film bearings have been carried out considering inertia, and turbulent effects to calculate and estimate the performance characteristics of them [7-9]. On the other hand, thermal influences on the lubrication is one of the important research topics, and in these studies, the static performance properties of the bearings such as the pressure and temperature distributions of the lubrication film, the load carrying capacity, power consumptions etc. were numerically and experimentally investigated in detailed [10-12]. Moreover, the researchers were analyzed the effects of the variable viscosity on these performance characteristic for different bearing types such as thrust, journal, and pad, different bearing geometry such as circular, lobe, and elliptical, as well as considering manufacturing errors and/or modifications such as surface roughness and texture, and misalignment etc., and they concluded that the rise in the temperature strongly affected the static performance characteristics of the bearings under operating with heavy loads [13-17].

The stability of the shaft-bearing system strongly relates with the damping characteristics, as well as stiffness coefficients that are known as dynamic characteristics [18]. In literature, these characteristics, as well as the stability of the system have been carried out in many studies in isothermal condition. In these studies, the methods that are preferred to investigate the stability of the system could be categorized two main approaches as perturbation analysis and the steady-state analysis of the response. Klit and Lund [19] analyzed the lubrication problem with the perturbation method, and they calculated stiffness and damping coefficients by solving Reynolds equation. Rao and Sawicki [20] studied linear stability of the system, in addition, they computed the dynamic characteristics of the bearing considering cavitation effects. They researched the cavitation effects on the stability. Majumdar [21] also modeled perturbed Reynold's equation to obtain the dynamic coefficients and investigated the stability of the system. Pai et. al. [22] carried out a stability analysis with perturbation method for a three lobes hydrodynamic journal bearing, and they calculated the stiffness and damping characteristics. On the other hand, there are few researches on the investigation of the dynamic coefficients under the thermal influences. Nagaraju et al. [23] researched a two-lobe journal bearing under thermal effects. They modeled the lubricant temperature with 2-dimensional energy equation, then they determined the performance characteristics such as attitude angle, load capacity, etc., in addition, they also calculated the dynamic parameters such as threshold speed, critical mass, and whirl frequency. Xu et. al., [24] investigated the bearing characteristics considering variable viscosity and

turbulent conditions. They modeled the temperature distribution with 2-dimensional energy equation. They derived the damping and stiffness coefficients from the load capacity, and they researched the influences of the misalignment on the dynamic and static performance characteristics for different eccentricity ratios. Shi et. al., [25] experimentally and numerically researched the dynamic characteristics of the coupled thrust and journal bearing. Based on perturbation analysis, they investigated the variations of the damping and stiffness coefficients considering thermal effects for different surface texture patterns, as well as different radial clearance values.

A comprehensive literature review shows that the dynamic and performance characteristics are affected by the lubricant temperature. Although numerical and experimental analyses of the static performance characteristics were carried out in many studies by considering the thermal effects, there is a limited number of researches on the dynamic characteristics. In these studies, the temperature variations along film thickness direction were generally ignored (2-dimensional energy equation), moreover, whereas the eccentricity ratio influences on the dynamic characteristics were studied, the variations of the dynamic characteristics concerning the shaft speed weren't investigated in detailed. Recently, high-speed rotor-bearing systems such as turbocharger, spindle etc. have commonly used in several machines and/or mechanical systems, and identifying safe working conditions is crucial by designing and analyzing the bearing considering thermal effects. This study mainly focused on the investigation of the damping and stiffness characteristics of a shaft-bearing system and the stability analysis considering thermal effects. In this study, by taking into consideration variable viscosity, to compute the dynamic parameters of the shaft-bearing system, the lubricant flows, as well as the heat transfers between lubricant and the journal, as well as between shaft and lubricant were modelled with Dowson equation and 3-dimensional energy equation, and heat conduction equation, respectively. Then, the perturbation pressure equations were derived from the Dowson equation for a two-degree-of-freedom system. And this lubrication model was simultaneously solved with finite difference scheme and successive over relaxation methods. Finally, a serial simulation was carried out under different shaft speed to investigate the stability parameters and the variations of the dynamic coefficients for different radial clearance values.

2. THEORETICAL MODELS

In the bearing-shaft system supported by fluid-film bearings, pressure force acting on the shaft surface determines the dynamic characteristics. On the other hand, this force directly depends on the viscosity of the lubricant affected by heat generation in the system. Therefore, to investigate the dynamic characteristics of the system, firstly the lubricant flow between shaft and

journal surfaces was modelled under variable viscosity, and then the mathematical models were derived for heat transfer between lubricant and journal, as well as journal surface and environment.

2.1. Dowson's Equation

Figure 1 shows views of a shaft supported by a hydrodynamic journal bearing. To obtain the pressure distribution function of the lubricant, its flow through radial clearance could be modelled by governing of the equations of motions, in other words Navier Stokes equations. According to theory of hydrodynamic lubrication for an incompressible fluid, the flow of the lubricant could be modeled with Dowson's equation under variable viscosity, and a dimensionless form of Dowson's equation could be written as Eq. 1 for variable viscosity and cylindrical coordinate system. In the equation, the dimensionless parameters and viscosity terms are given in Eq. 2 and Eq. 3, respectively.

$$\theta = x/R, \quad \xi = y/R, \quad \bar{h} = h/c, \quad (2)$$

$$\Omega = \left(\frac{\omega\mu}{P_s}\right) (R/c)^2, \quad \bar{z} = z/\bar{h}$$

$$\bar{\mu} = \mu/\mu_0, \quad F_0 = \int_0^1 \frac{d\bar{z}}{\bar{\mu}}, \quad F_1 = \int_0^1 \frac{\bar{z}d\bar{z}}{\bar{\mu}} \quad (3)$$

In Dowson's equation, \bar{h} denotes the dimensionless film thickness function. When the shaft oscillates in the

$$\frac{\partial}{\partial\theta} \left(\bar{h}^3 \left(\int_0^1 \frac{\bar{z}}{\bar{\mu}} \left(\bar{z} - \frac{F_1}{F_0} \right) d\bar{z} \right) \frac{\partial \bar{p}}{\partial\theta} \right) + \frac{\partial}{\partial\xi} \left(\bar{h}^3 \left(\int_0^1 \frac{\bar{z}}{\bar{\mu}} \left(\bar{z} - \frac{F_1}{F_0} \right) d\bar{z} \right) \frac{\partial \bar{p}}{\partial\xi} \right) = \Omega \frac{\partial}{\partial\theta} \left[\bar{h} - \left(\bar{h} \frac{F_1}{F_0} \right) \right] \quad (1)$$

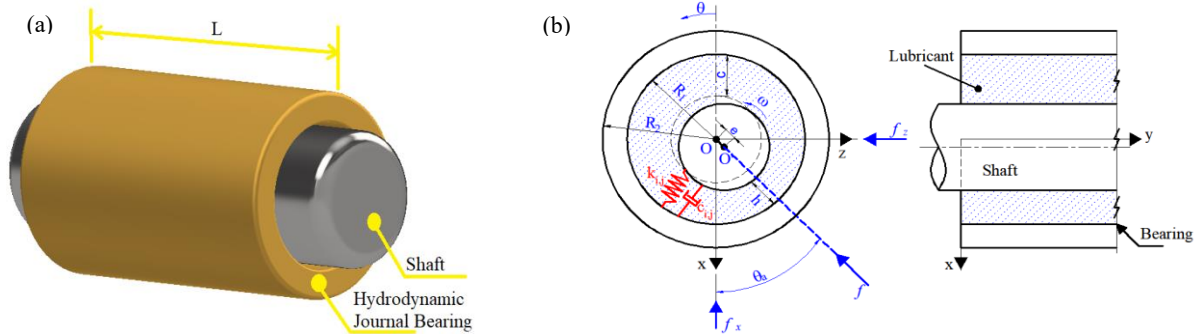


Figure 1. Schematic view and coordinate axis

$$\frac{\partial}{\partial\theta} \left(\bar{h}_0^3 F_2 \frac{\partial \bar{p}_\beta}{\partial\theta} \right) + \frac{\partial}{\partial\xi} \left(\bar{h}_0^3 F_2 \frac{\partial \bar{p}_\beta}{\partial\xi} \right) = \Omega \left[\frac{\partial \bar{h}_0}{\partial\theta} - \frac{\partial}{\partial\theta} \left(\bar{h}_0 \frac{F_1}{F_0} \right) \right], \quad \beta = 0$$

$$= \begin{cases} -\frac{\partial}{\partial\theta} \left(3\bar{h}_0^2 F_2 \frac{\partial \bar{p}_0}{\partial\theta} \cos\theta \right) - \frac{\partial}{\partial\xi} \left(3\bar{h}_0^2 F_2 \frac{\partial \bar{p}_0}{\partial\xi} \cos\theta \right) + \Omega \left[-\sin\theta - \bar{h}_0 \frac{\partial}{\partial\theta} \left(\frac{F_1}{F_0} \right) + \sin\theta \left(\frac{F_1}{F_0} \right) \right], & \beta = x \\ -\frac{\partial}{\partial\theta} \left(3\bar{h}_0^2 F_2 \frac{\partial \bar{p}_0}{\partial\theta} \sin\theta \right) - \frac{\partial}{\partial\xi} \left(3\bar{h}_0^2 F_2 \frac{\partial \bar{p}_0}{\partial\xi} \sin\theta \right) + \Omega \left[\cos\theta - \bar{h}_0 \frac{\partial}{\partial\theta} \left(\frac{F_1}{F_0} \right) + \cos\theta \left(\frac{F_1}{F_0} \right) \right], & \beta = y \\ \cos\theta, & \beta = \dot{x} \\ \sin\theta, & \beta = \dot{y} \end{cases} \quad (7)$$

$$F_2 = \int_0^1 \frac{\bar{z}}{\bar{\mu}} \left(\bar{z} - \frac{F_1}{F_0} \right) d\bar{z} \quad (8)$$

journal bearing around its equilibrium position in x and z axis, a small perturbation is generated. Therefore, the dimensionless film thickness function could be computed from Eq. 4.

$$\bar{h} = \bar{h}_0 + \Delta x \cos\theta + \Delta z \sin\theta \quad (4)$$

In the perturbed film thickness, Δx and Δz are small perturbations along x and z directions. \bar{h}_0 denotes the dimensionless thickness function at the equilibrium position of the shaft, and it could be modelled as Eq. 5.

$$\bar{h}_0 = 1 + \varepsilon \cos(\theta - \theta_a) \quad (5)$$

where ε and θ_a express the eccentricity ratio and the attitude angle, respectively. For a small perturbation motion of the shaft around its equilibrium position, the lubricant pressure in the radial clearance could be expressed in Eq. 6 by expanding with Taylor series of displacements and velocities [18].

$$\bar{p} = \bar{p}_0 + \Delta x \bar{p}_x + \Delta y \bar{p}_y + \Delta \dot{x} \bar{p}_{\dot{x}} + \Delta \dot{y} \bar{p}_{\dot{y}} \quad (6)$$

where \bar{p}_0 represents the steady state pressure, and \bar{p}_β ($\beta = x, y, \dot{x}, \dot{y}$) denotes the perturbed pressure of the lubricant. The steady-state and perturbed pressures of the lubricant could be derived from Dowson's equation by neglecting higher-order terms, and they could be expressed in Eq. 7. F_2 could be given in Eq. 8.

The boundary conditions of the steady-state pressure and the perturbed pressure equations could be defined in Eq. 9 for a shaft supported by hydrodynamic journal bearing.

$$\begin{aligned} \xi = 0 \text{ and } \xi = 1, \quad \bar{p}_0 = \bar{p}_\beta = \bar{p}_a \\ \theta + 2\pi, \begin{cases} \bar{p}_0(\xi, \theta) = \bar{p}_0(\xi, \theta + 2\pi) \\ \bar{p}_\beta(\xi, \theta) = \bar{p}_\beta(\xi, \theta + 2\pi) \end{cases} \end{aligned} \quad (9)$$

2.2. Heat Transfer in Bearing-Shaft System

When the shaft-bearing system operates, heat transfer from the lubricant to shaft and journal will be existed due to friction between the lubricant layer and/or heat flux from hot to cold media. And as expected, the lubricant viscosity will change during operation due to these heat transfer mechanisms. The heat transfer could be modelled both in fluid layers and through solid surface, as well as their interfaces. In this study, the temperature distributions of the lubrication film and the journal structure were modelled with the 3-dimensional energy equation and heat conduction equation, respectively. 3-dimensional energy equation in dimensionless form could be written as Eq. 10 for a cylindrical geometry [26-27].

$$\begin{aligned} \bar{h}^2 \left(\bar{u} \frac{\partial \bar{T}_L}{\partial \theta} + \bar{v} \frac{\partial \bar{T}_L}{\partial \xi} + \frac{\bar{w}}{h} \frac{\partial \bar{T}_L}{\partial \bar{z}} - \bar{u} \frac{\bar{z}}{h} \frac{\partial \bar{h}}{\partial \theta} \frac{\partial \bar{T}_L}{\partial \bar{z}} \right) \\ = P_e \frac{\partial^2 \bar{T}_L}{\partial \bar{z}^2} + D_e \bar{\mu} \left[\left(\frac{\partial \bar{u}}{\partial \bar{z}} \right)^2 + \left(\frac{\partial \bar{v}}{\partial \bar{z}} \right)^2 \right] \end{aligned} \quad (10)$$

where \bar{T}_L denotes the dimensionless lubricant temperature, \bar{u} , \bar{v} , and \bar{w} express the dimensionless velocity components along x, y, and z coordinates, respectively. They could be derived from pressure distribution and continuity equation. P_e and D_e are Peclet and dissipation numbers, and they could be computed from Eq. 11.

$$P_e = \frac{k_L \mu_0}{C_L \rho_L p_a} \left(\frac{R}{c^2} \right)^2 \quad D_e = \frac{p_a}{C_L \rho_L T_0} \quad (11)$$

The velocity components, \bar{u} and \bar{v} could be computed from Eq. 12 and Eq. 13, and \bar{w} could be calculated with continuity equation given in Eq. 14.

$$\bar{u} = \left(\int_0^{\bar{z}} \bar{h}^2 \frac{d\bar{z}}{\bar{\mu}} \right) \left(\frac{\Omega}{F_0} - \frac{F_1}{F_0} \frac{\partial \bar{p}}{\partial \theta} \right) + \frac{\partial \bar{p}}{\partial \theta} \int_0^{\bar{z}} \bar{h}^2 \frac{\bar{z} d\bar{z}}{\bar{\mu}} \quad (12)$$

$$\bar{v} = \frac{\partial \bar{p}}{\partial \xi} \left(\int_0^{\bar{z}} \bar{h}^2 \frac{\bar{z} d\bar{z}}{\bar{\mu}} \right) \left(1 - \frac{F_1}{F_0} \right) \quad (13)$$

$$\frac{\partial \bar{u}}{R \partial \theta} + \frac{\partial \bar{v}}{R \partial \xi} + \frac{\partial \bar{w}}{c \bar{h} \partial \bar{z}} = 0 \quad (14)$$

In the Eq. 10, the Vogel viscosity-temperature relation model is given in Eq. 15.

$$\bar{\mu} = e^{-\eta(\bar{T}_L - 1)} \quad (15)$$

where η represents a coefficient, and it equals 0.034 for commercial oil. On the other hand, the temperature distribution of the journal can be derived for heat conduction and, it can be written as Eq. 16 in cylindrical coordinates.

$$\frac{1}{\bar{r}^2} \frac{\partial^2 \bar{T}_J}{\partial \theta^2} + \frac{\partial^2 \bar{T}_J}{\partial \xi^2} + \frac{1}{\bar{r}} \frac{\partial \bar{T}_J}{\partial \bar{r}} + \frac{\partial^2 \bar{T}_J}{\partial \bar{r}^2} = 0 \quad (16)$$

where \bar{T}_J represents the dimensionless journal temperature, and \bar{r} is cylindrical coordinate through journal radius. With regards to the system geometry, the boundary conditions at the interfaces between lubricant and solid surfaces, as well as the environment could be listed as following.

- At the interface between the lubricant and shaft surface, $\bar{T}_L(\theta, \xi, \bar{z} = 1) = \bar{T}_s$
- At the interface between the lubricant and journal surface,

$$-\frac{k_J}{R} \frac{\partial \bar{T}_J}{\partial \bar{r}} \Big|_{\bar{r}=0} = \frac{k_L}{c \bar{h}} \frac{\partial \bar{T}_L}{\partial \bar{z}} \Big|_{\bar{z}=0}$$

- At the lateral surfaces of the journal, the heat transfers between lateral surfaces of the journal and air

$$-\frac{k_J}{R_J} \frac{\partial \bar{T}_J}{\partial \bar{r}} \Big|_{\bar{r}=R_2} = -h_J(\bar{T}_J - \bar{T}_a)$$

- At the outer surface of the journal, the heat transfers between surface and air;

$$-\frac{k_J}{R_2} \frac{\partial \bar{T}_J}{\partial \xi} \Big|_{\xi=0 \text{ and } 1} = -h_J(\bar{T}_J - \bar{T}_a)$$

2.3. Dynamics Coefficients and Performance Characteristics

The dynamics coefficients and the performance characteristics of the hydrodynamic journal bearing could be calculated from the steady-state and perturbed pressure distribution obtained with an iterative solution of Eq. 1 and Eq. 7. The power loss that is one of the performance characteristics of the bearing could be computed from friction forces obtained with integrating of the shear stress. The friction force and the power loss could be calculated from Eq. 17 and Eq. 18, respectively.

$$\bar{F}_f = \int \int \left(\frac{\bar{h} \partial \bar{p}_0}{\partial \theta} - \frac{\bar{h} F_1}{F_0} + \frac{\Omega}{\bar{h} F_0} \right) d\theta d\xi \quad (17)$$

$$\bar{P}_f = \bar{F}_f \omega R \quad (18)$$

The stiffness and the damping coefficients along x and y directions could be obtained from perturbed pressure distributions. The direct (\bar{k}_{xx} and \bar{k}_{yy}) and coupled (\bar{k}_{xy} and \bar{k}_{yx}) stiffness coefficients could be calculated with integrating of perturbed pressure distribution related with displacement, \bar{p}_x and \bar{p}_y , while the direct (\bar{c}_{xx} and \bar{c}_{yy}) and coupled (\bar{c}_{xy} and \bar{c}_{yx}) damping coefficients could be calculated with integrating of the perturbed pressure distribution related with velocity, \bar{p}_x and \bar{p}_y . These coefficients could be given in Eq. 19 and Eq. 20.

$$\bar{K} = \begin{bmatrix} \bar{k}_{xx} & \bar{k}_{xy} \\ \bar{k}_{yx} & \bar{k}_{yy} \end{bmatrix} = \int \int \begin{bmatrix} -\cos\theta \\ -\sin\theta \end{bmatrix} [\bar{p}_x \quad \bar{p}_y] d\theta d\xi \quad (19)$$

$$\bar{C} = \begin{bmatrix} \bar{c}_{xx} & \bar{c}_{xy} \\ \bar{c}_{yx} & \bar{c}_{yy} \end{bmatrix} = \int \int \begin{bmatrix} -\cos\theta \\ -\sin\theta \end{bmatrix} [\bar{p}_x \quad \bar{p}_y] d\theta d\xi \quad (20)$$

2.4. Equations of Motions and Stability Analysis

The equations of motions could be derived as Eq. 21 in a dimensionless form for a rigid shaft supported by a single hydrodynamic journal bearing.

$$\begin{bmatrix} m & 0 \\ 0 & m \end{bmatrix} \begin{bmatrix} \ddot{x} \\ \ddot{y} \end{bmatrix} + \begin{bmatrix} \bar{c}_{xx} & \bar{c}_{xy} \\ \bar{c}_{yx} & \bar{c}_{yy} \end{bmatrix} \begin{bmatrix} \dot{x} \\ \dot{y} \end{bmatrix} + \begin{bmatrix} \bar{k}_{xx} & \bar{k}_{xy} \\ \bar{k}_{yx} & \bar{k}_{yy} \end{bmatrix} \begin{bmatrix} x \\ y \end{bmatrix} = 0 \quad (21)$$

The homogenous solution of Eq. 21 could be assumed to be an exponential function, then the eigenvalue of the Eq. 18 and characteristic equations could be obtained. Then the stability parameters, in other words, the critical mass, M_{cr} , and whirl frequency ratio, γ could be derived as Eq. 22 and Eq. 23, respectively (as similar to [3, 29]).

$$M_{cr} = \frac{K_e}{\gamma^2} \quad (22)$$

$$\gamma = \sqrt{\frac{(K_e - k_{xx})(K_e - k_{yy}) - k_{xy}k_{yx}}{c_{xx}c_{yy} - c_{xy}c_{yx}}} \quad (23)$$

In Eq. 22 and Eq. 23, K_e represents the equivalent stiffness coefficient and it could be computed as following.

$$K_e = \frac{k_{xx}c_{yy} + k_{yy}c_{xx} - k_{xy}c_{yx} - k_{yx}c_{xy}}{c_{xx} + c_{yy}} \quad (24)$$

3. NUMERICAL SOLUTION AND MODEL VERIFICATION

The performance characteristics and dynamic coefficients of the journal bearing-shaft system directly depend on the lubricant pressure in the radial clearance. Moreover, due to the variation of lubricant viscosity concerning the temperature, as well as heat generation in solid surfaces (bearing and shaft surfaces), the characteristics of the bearings such as pressure distribution, must be evaluated with the temperature. Therefore, an algorithm was developed to solve the mathematical models, simultaneously. This numerical solution algorithm starts with input parameters such as dimensions and operating conditions of the system, and

it follows step-by-step iterative solution procedure listed as below.

- Step 1: Initial conditions of the pressure in the radial clearance and temperatures of the lubricant, journal, and shaft are defined.
- Step 2: The initial viscosity distribution and film thickness are computed.
- Step 3: The steady-state, perturbed pressure distributions (Eq. 7), and total pressure distribution (Eq. 6) are computed with numerical solution of perturbed Dowson's equation based on an iterative solution. Then, computed the velocity components from pressure distribution (Eq. 12-Eq. 14).
- Step 4: The temperature distributions of the lubricant and journal are obtained with numerical solution of the 3-dimensional energy equation and heat conduction equation, simultaneously.
- Step 5: For this new temperature distribution of the lubricant, the viscosity distribution is obtained from viscosity-temperature relation model
- Step 6: Repeat the solution procedure from Step 3 to Step 5 until the convergence about the viscosity distribution is achieved
- Step 7: Computed the performance characteristics and dynamic coefficients, as well as stability parameters.

In the solution of the models, the finite difference method combined with successive over relaxations is preferred to obtain pressure and temperature distributions. And the pressure distribution is calculated on a MxN solution mesh in circumferential and axial directions, while the temperature and the viscosity distributions are computed on a MxNxZ resolution mesh in circumferential, axial, and radial (along film thickness and bearing radius) directions. Because the numerical solutions of the temperature, viscosity, and pressure distributions are sensitive the mesh size and density, a mesh independency study was performed. To ensure the convergence, as well as to obtain an efficient solution for computation time, the number of the grid nodes, M, N, Z, are preferred as 48, 156, and 24, respectively.

Table 1. Operating conditions and geometry of the bearing-shaft system [16, 28]

Parameters	Symbol	Value
Ambient Temperature	T_a	40 °C
Oil Viscosity	μ	0.0277 Pa. s
Density	ρ	860 kg / m ³
Specific heat of the lubricant	C_L	2000 J / kg . °C
Thermal conductivity of the lubricant	k_L	0.13 W / m °C
Bearing inner radius,	R_1	50 mm
Bearing outer radius,	R_2	75 mm
Bearing length	L	80 mm
Thermal Conductivity of the bearing	k_J	250 W / m °C
Heat transfer coefficient of the bearing	h_J	80 W / m ² °C

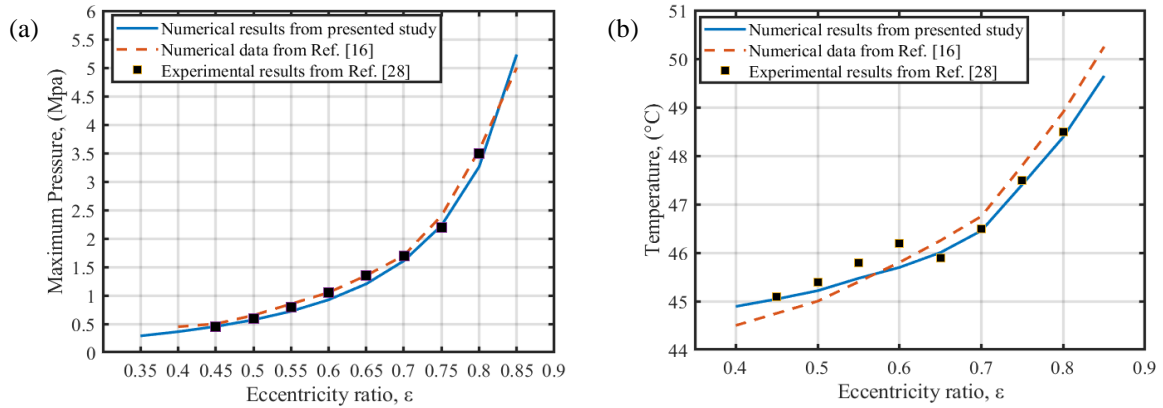


Figure 2. Comparison of the simulation results and published experimental and numerical data, a) maximum pressure, b) maximum temperature ($c=145 \mu\text{m}$)

The simulation results obtained from numerical solution are compared to validate with an experimental data from Ref. [28] and a numerical data from Ref. [16]. In the validation study, the simulation was run under main parameters and the operating conditions listed in Table 1, and the maximum lubricant pressure and temperature values are computed for different eccentricity ratios. Fig 2a and Fig. 2b show the variations of the maximum pressure and temperature values concerning with the eccentricity ratio, respectively. It can be seen from Fig. 2a that the variations of the maximum pressure values with respect to eccentricity ratio are closer to both experimental and numerical data, and the results show a good agreement. Furthermore, when the eccentricity ratio is lower than 0.7, a deviation between test data and numerical results are occurred for the variations of the maximum temperature values. The results in the presented study show a better agreement.

4. RESULTS AND DISCUSSION

In this study, the variations of the stiffness and the damping coefficients concerning with the rotating speed are researched for different radial clearances. Therefore, the radial clearances of the bearings were chosen as $100 \mu\text{m}$, $125 \mu\text{m}$, and $150 \mu\text{m}$, and the performance characteristics and the dynamic coefficients were computed with the numerical solution algorithm under thermal and isothermal cases. And the variations of the performance characteristics and the dynamic coefficients with respect to the rotating speed are presented and discussed, and then the stability of the system is investigated. And, in the simulation, the bearing-shaft system whose geometry information of the system is listed in Table 1 operates at an eccentricity ratio, 0.5.

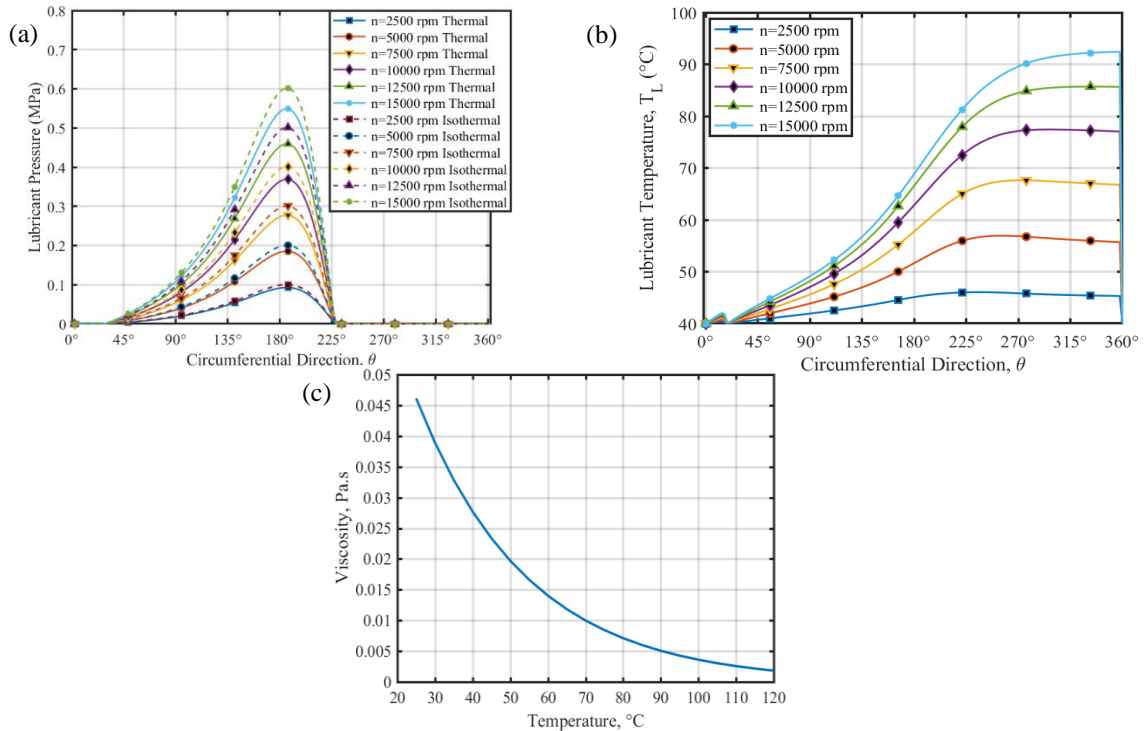


Figure 3. The pressure and temperature values of the lubricant along circumferential direction, and variations of the viscosity a) pressure b) temperature, ($c=100 \mu\text{m}$), and c) viscosity-temperature relationship

For the radial clearance of 100 μm , Fig. 3 shows the pressure and temperature values of the lubricant where is at $L/2$ along circumferential direction under different rotating speeds. Moreover, the effects of the temperature on the oil viscosity are illustrated in Fig. 3c. The pressure values around the bearing center ($\theta=180^\circ$) are higher than other region of the radial clearance due to eccentric position of the shaft in the journal, as expected, and this variation profile of the pressure are similar for each cases. However, when the rotating speed increases, the pressure values around the bearing center grow up due to rotation effect. On the other hand, although the peak pressure values are almost same for lower rotating speed under both thermal and isothermal cases, when the rotating speed grows up, the differences between the pressure values increase. While the peak pressure grows up 5.5 times for thermal cases, it grows up 6 times for the isothermal cases, when the shaft speed increases from 2500 rpm to 15000 rpm due to temperature influence on the oil viscosity (see Fig. 3c). Fig. 3b shows the variations of the temperature values at $L/2$ along the circumferential direction for different rotating speeds. Due to eccentric position of the shaft, as well as the direction of the angular speed, the temperature values in a range of circumferential direction between $\theta=180^\circ$ and $\theta=360^\circ$ are high, in addition, this temperature profile is similar for different rotating speeds. However, it is seen from Fig. 3b that the temperature values are higher for high rotating speeds. The temperature of the lubricant reaches 45 $^\circ\text{C}$ for bearing-shaft system under rotating speed of 2500 rpm, while it exceeds 90 $^\circ\text{C}$, when the rotating speed reaches 15000 rpm.

Fig. 4 shows variations of the peak pressure and the maximum temperature values of the lubrication film concerning of the shaft speed in thermal and isothermal cases. In both cases, the maximum pressure values grow up as shaft speed increases due to hydrodynamic effects on the pressure distribution. In addition, the maximum pressure values are high for small radial clearance at each case. However, the variations of the maximum pressure values with respect to shaft speed behaves linear increasing for isothermal cases, whereas the increasing in the maximum pressure in the thermal cases decelerates when the shaft speed rises up due to thermal effects. When the shaft speed increases from 7500 rpm to 15000 rpm, the maximum pressure for radial clearance of 100 μm , 125 μm , and 150 μm under isothermal cases grow up 50%, 48%, and 46%, respectively, whereas the temperature values under thermal cases increase by 36%, 40%, and 45%, respectively. It is seen from Fig. 4b that although the lubricant temperature values are nearly constant for slow rotational speed, the temperature values increase when the shaft speed rises by exceeding 2500 rpm. Therefore, the maximum pressure values decrease due to the viscosity-temperature relation when the shaft speed increases. Moreover, the maximum temperature of the radial clearance of 100 μm rises to 72 $^\circ\text{C}$, when the shaft speed reaches 15000 rpm. Since the temperature values variations with the shaft speed, it could be noted

that the maximum pressures diminish by 36%, 33%, and 23% for radial clearance 100 μm , 125 μm , and 150 μm , respectively, as the isothermal and thermal cases are compared.

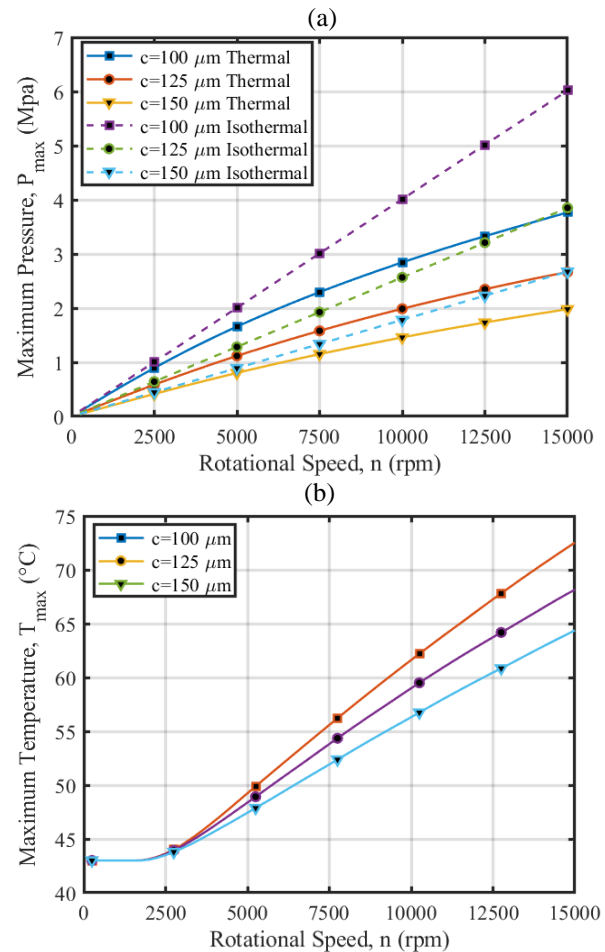


Figure 4. The variations of the peak pressure and the maximum temperature values of the lubricant with respect to the shaft speed, a) maximum pressure, b) maximum temperature

4.1. Performance Characteristics

The lubrication film and the friction forces, and the power consumption that are called the performance characteristics of the bearing were computed with the numerical solution algorithm for difference radial clearance under thermal and isothermal cases, and the variations of the performance characteristics with respect to the shaft speeds were illustrated in Fig. 5 for each case. It is seen from Fig. 5a that when the shaft speed rises up, the film force increases for both thermal and isothermal cases due to hydrodynamic effect on the pressure distribution. In addition, because, the radial gap affects the squeezing of the lubricant, the lubrication film forces grow up, as the radial clearance becomes small, as expected. On the other hand, the film forces almost linearly increase for isothermal cases, whereas for the thermal cases, the increase in the forces starts to be slowdown when the shaft speed rises up. At the journal bearing-rotor system run under 15000 rpm, the film force reaches to a maximum value of 30 kN for isothermal case

and radial clearance of 100 μm . When the thermal effects taken into account for same radial clearance, the force decreases by 33%, and it nearly equals to 20 kN. In addition, the difference between the thermal and isothermal cases decreases as the radial clearance increases. Because, the film force, in other words, load capacity, directly depends on the viscosity of the lubricant that decays with the temperature rising, as expected the lubrication film forces decrease, also. On the other hand, Fig. 5b and Fig. 5c show the variations of the friction force and power consumption with respect to the shaft speed. While the friction forces nearly linear increase with shaft speeds for isothermal cases, they exponentially vary with shaft speed for the thermal cases. In addition, as similar to characteristic of the film force, the friction force is higher for small radial clearance. When the radial clearance grows up from 100 μm to 150 μm , the friction force decreases by maximum of 34% in the isothermal case, while it decreases by 20% in the thermal case. In addition, the friction force is maximum for 15000 rpm and radial clearance of 100 μm for each case, but it reaches to 640 N for isothermal cases, whereas the friction force decreases by 45%, when the thermal effects take into account. In journal bearings, the power consumption defines the necessary power to overcome the friction.

Therefore, the friction force directly determines the power consumption. It is seen from Fig. 5c that the power consumption is higher for isothermal cases, and it increases when the shaft speed increases. In addition, the power consumption is high for small radial clearance. In addition, for the radial clearance of 100 μm , when the thermal effects take into account, the decreasing in the power consumption is maximum, and it is nearly to be 45%. For high shaft speed, because the temperature of the lubricant rises up to 70 $^{\circ}\text{C}$ (see Fig. 4b), the viscosity of the lubricant decay, as well as the friction between the layers of the fluid. Therefore, although the friction forces and thus power consumptions are increase when the shaft speed rises up, they strongly affect by the temperature of the lubricant.

4.2. Dynamic Coefficients

In journal bearing-shaft system, the lubricant behaves like a spring, as well as a damping characteristic when it flows into radial gap. Because it directly supports the shaft, the stiffness and damping characteristics are crucially important to the stability of the system. To investigate dynamic coefficients of the bearing under variable viscosity, the damping and the stiffness coefficients are computed for different radial clearances in the thermal and isothermal cases.

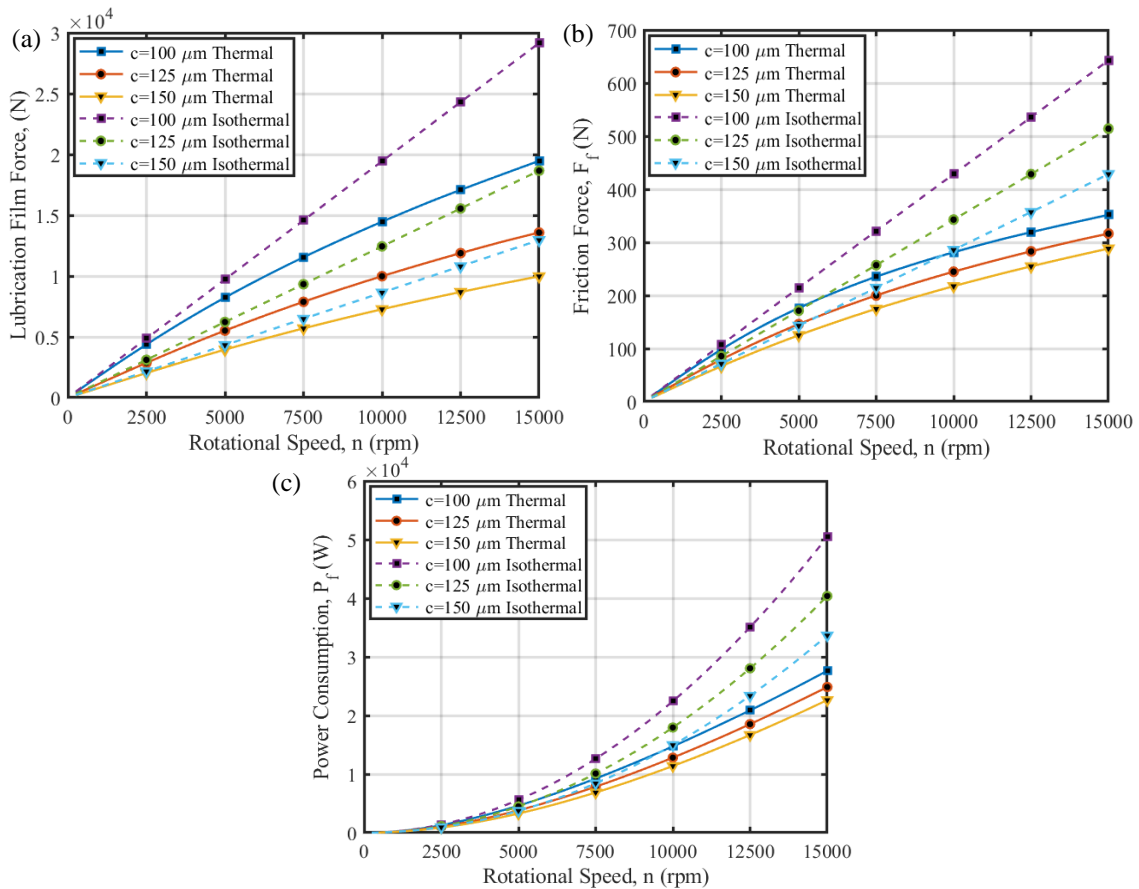


Figure 5. The variations of the performance characteristics with respect to the shaft speed, a) lubricant film force, b) friction force, c) power consumption

Fig. 6 shows the variations of the direct and cross stiffness of the hydrodynamic journal bearings with

respect to the shaft speed. When the thermal effects are taken into account, the stiffness coefficients decrease due

to decay in the viscosity, as expected. In addition, because the radial clearance determines the squeezing on the pressure values, and so the film forces the hydrodynamic bearings whose small radial clearance have high stiffness coefficients in both cases. Moreover, when the shaft speed increases, the stiffness coefficients, k_{xx} , k_{yy} , and k_{yx} positively grows up, whereas the stiffness coefficient, k_{xy} increases negatively. On the other hand, as similar to the characteristics of the load capacity variations, for isothermal cases, the coefficient variations are almost linear, whereas the variations are non-linear for thermal cases due to the shaft speed influences on the temperature. For the same shaft speeds, the cross stiffness coefficients, k_{xy} are the highest due to eccentricity direction, as expected, and the lowest stiffness coefficients are k_{yy} . In addition, the difference between thermal and isothermal cases varies for each coefficient, as well as the radial clearance.

To discuss the thermal effects on the stiffness, the percentage differences are computed for shaft speed of 15000 rpm, and are presented in Table 2. The thermal effect on the stiffness coefficient is more dominant for k_{yy} , while this effect is least for k_{yx} among the stiffness coefficients. On the other hand, it could be said that the thermal effect on the stiffness coefficient becomes weak when the radial clearance grows up. The radial clearance determines the hydrodynamic boundary layer between the shaft and journal surfaces, and the rise in the temperature of the lubricant becomes low for high radial clearance values. Furthermore, the temperature directly depends on the lubricant velocity, in other words the lubricant pressure. And, the pressure values decrease due to a weak squeezing effect on the lubricant when the radial clearance increases, and the components of the velocity are also decrease.

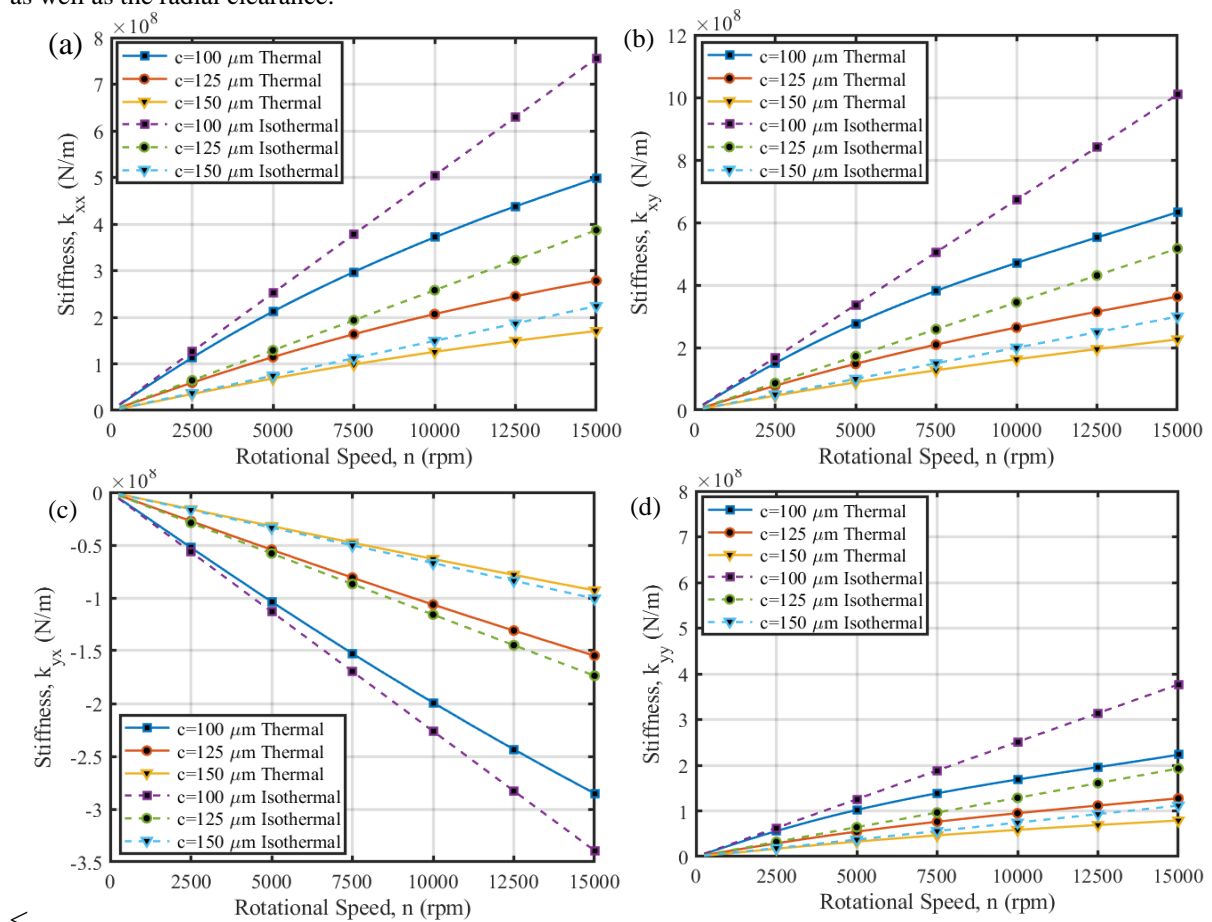


Figure 6. The variations of stiffness coefficients of the bearing-shaft system with respect to the shaft speed, a) k_{xx} , b) k_{xy} , c) k_{yx} , d) k_{yy}

Table 2. The percentage difference between thermal and isothermal cases

Radial Clearance, c (μm)	Stiffness Coefficient			
	k_{xx}	k_{yy}	k_{xy}	k_{yx}
100	33.3	42.1	38	17.6
125	28.2	40	30	14.2
150	24	28.5	26.6	12

Fig. 7 shows the variations of the direct and cross damping coefficients concerning the shaft speed. When the shaft speed grows up, the damping coefficients are almost constant in isothermal cases, whereas the damping coefficients decrease for thermal cases. Because the temperature rises due to high rotational speed, the viscosity decay, and thus the damping coefficients decrease. In addition, the direct damping coefficients, c_{xx} and c_{yy} are higher than the cross damping coefficients, c_{xy} and c_{yx} for each radial clearance in both cases. Moreover, the direct damping coefficients, c_{xx} and c_{yy} almost equal in the same parameters due to the symmetric structure of the bearing in isothermal cases. As similar to the direct damping coefficient, the cross damping coefficients, c_{xy} and c_{yx} are nearly the same, also. However, as the thermal

effects are taken into account, although the c_{xx} is higher than c_{yy} in the same parameters, c_{xy} and c_{yy} approximately equal. On the other hand, the thermal effects on the damping distinguish for each radial clearance, as well as direct and cross damping coefficients. To evaluate and discuss the thermal effects on the damping coefficients, the percentage differences are computed for the shaft speed of 15000 rpm, and the results are presented in Table 3. The thermal effect on the damping coefficient is more dominant for cross damping coefficients in low radial clearance, while this effect is least for c_{xx} among the coefficients. On the other hand, it could be said that the thermal effect on the damping coefficient becomes weak as the clearance grows up, because the temperature is low for small radial clearance (see Fig. 4b).

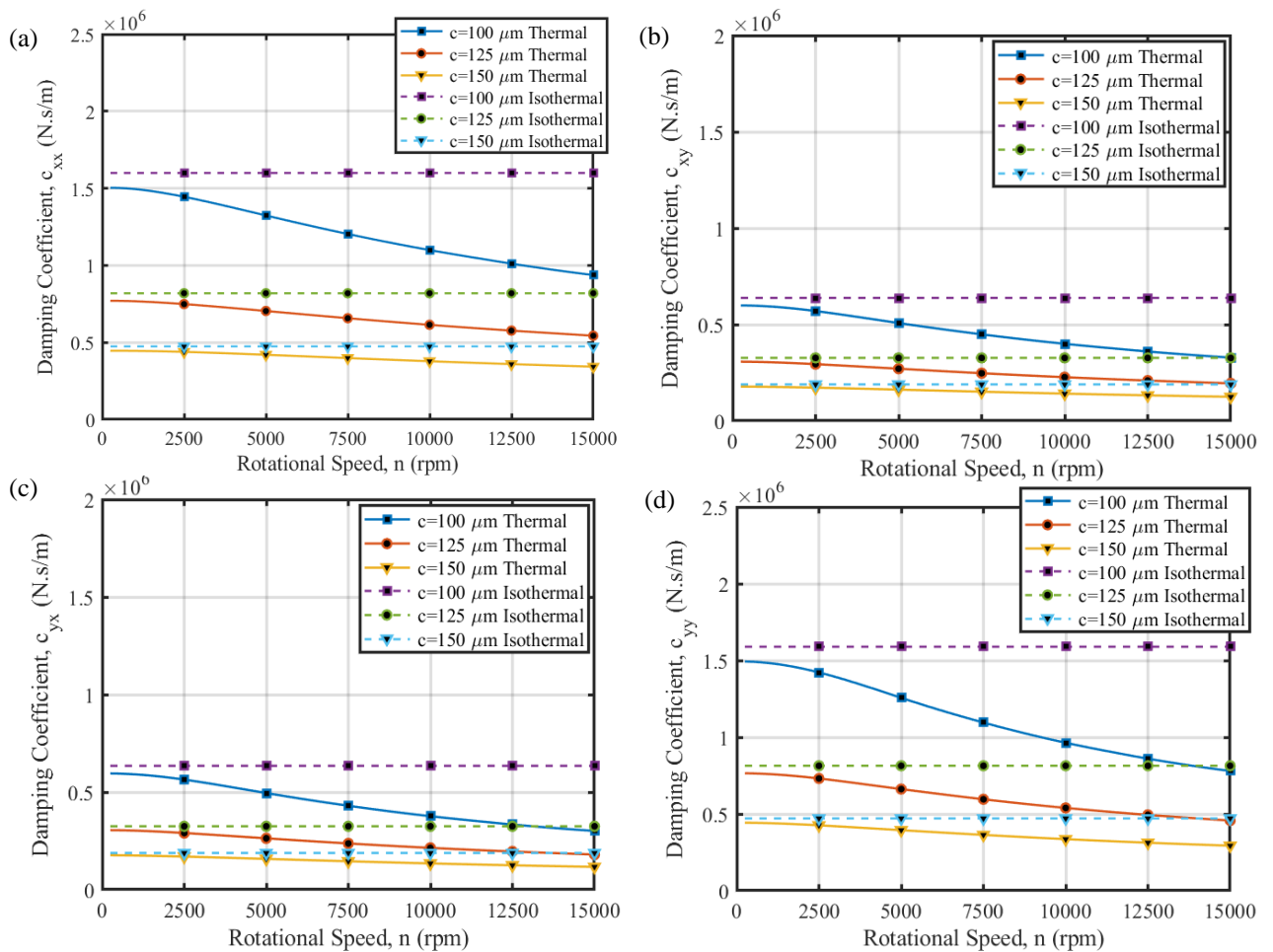


Figure 7. The variations of damping coefficients of the bearing-shaft system with respect to the shaft speed, a) c_{xx} , b) c_{xy} , c) c_{yx} , d) c_{yy}

Table 3. The percentage difference between thermal and isothermal cases

Radial Clearance, c (μm)	Damping Coefficient			
	c_{xx}	c_{yy}	c_{xy}	c_{yx}
100	43.2	53.9.1	55.8	56.2
125	31.2	38.7	38	34
150	29.3	38.5	37.5	33.3

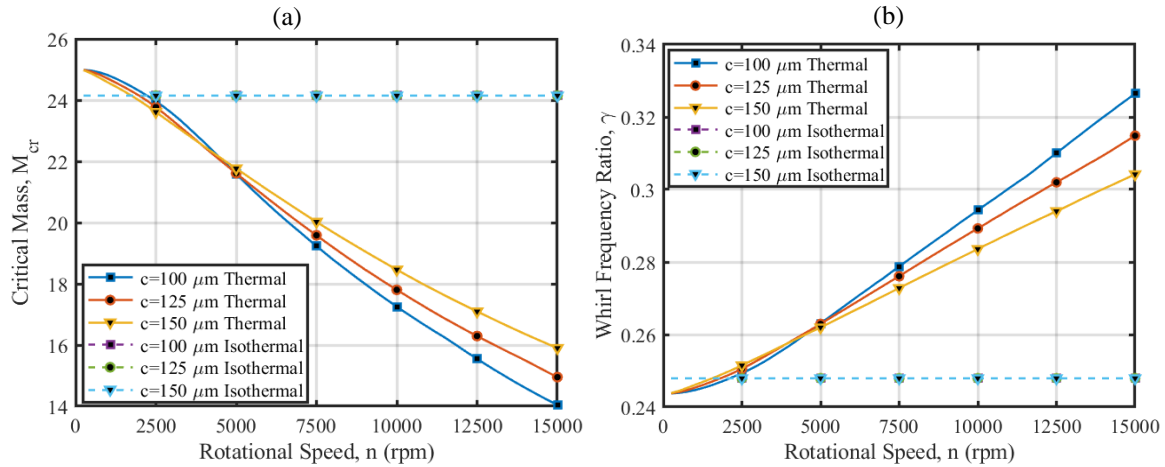


Figure 8. The variations of stability parameters of the bearing-shaft system with respect to the shaft speed, a) critical mass, b) whirl frequency ratio

4.3. Stability of The Bearing-Shaft System

The stability of the shaft supported by hydrodynamic journal bearing could be evaluated on the critical mass and whirl frequency ratio computed from the damping and stiffness coefficients. Fig. 8a shows the variations of critical mass of the system concerning the shaft speed. In the isothermal cases, the critical mass curves of the radial clearances are almost same, and these curves are approximately coincident. Therefore, the radial clearance, as well as the shaft speed, has little influence on the stability, when the thermal effects are neglected. Furthermore, when the thermal influence is taken into account, the critical mass affects by the radial clearance and the shaft speed. It is seen from Fig. 8a that the critical mass decreases as the shaft speed rises up. Moreover, when the system runs at low speed ($n < 5000$ rpm), the critical mass is high for big radial clearance. However, when the shaft speed exceeds 5000 rpm, the critical mass also increases with decrease the radial clearance. Besides, the area where is below the critical mass curves defines the stable region of the system. Therefore, the stable regions of the isothermal cases are wider than the stable regions of the thermal cases, as expected. Because the temperature rises due to shaft speed, viscosity of the lubricant decreases. The dynamic characteristics of the system affect by temperature rising, and the stable region of the system becomes narrow, as expected. Furthermore, the stable region becomes wide when the radial clearance increases, because the temperature rising has low effect on the dynamic coefficients for big radial clearance.

The whirl frequency ratio to be one of the stability parameters is the ratio between the whirl frequency and operating speed frequency. Fig. 8b shows the variations of the whirl frequency ratio concerning shaft speed for different radial clearance in both cases. As similar to variations of the critical mass, in the isothermal cases, the whirl frequency ratio curves of the radial clearances are approximately coincident, and the whirl frequency ratio values are almost constant in the shaft speeds. However, the whirl frequency ratio values in the thermal cases rise

up as the shaft speed increases. But, the whirl frequency ratios of the radial clearances are nearly the same for low speed ($n < 5000$ rpm). However, when the shaft speed exceeds 5000 rpm, the difference between the curves is distinguished, and the system supported by a bearing with small radial clearance has high whirl frequency ratio.

5. CONCLUSION

In this study, a shaft supported by a hydrodynamic journal bearing was evaluated considering temperature-viscosity relation, and the dynamic coefficients and performance characteristics of the shaft-hydrodynamic journal bearing system were numerically investigated in different shaft speeds, and radial clearance values. It is concluded that the temperature of the lubricant significantly rises at high shaft speed, and therefore the film forces, friction forces, and power consumption of the bearing decrease. Furthermore, effects of the variable viscosity on the performance are lower as the radial gap increases. On the other hand, when the shaft speed rises up, the direct and cross stiffness coefficients grow up in both cases. However, the direct and cross damping coefficients in thermal cases decrease, while they in isothermal cases approximately constant. Nevertheless, the dynamic coefficients in the thermal cases are lower, and the stiffness and damping coefficients decrease maximum 40% and 56%, respectively. Besides, thermal influence on the dynamic coefficients is more dominant for small radial clearance. In addition, it is drawn from the results that the variable viscosity strongly affects the stable region of the bearing-shaft system, and the critical mass decreases as the shaft speed grows, whereas the whirl frequency ratio increases. Besides, the thermal effects have more obvious influence on the stability of the shaft-bearing system with small radial clearance, however, the thermal effects on the stability, as well as the dynamic characteristics become weak when the shaft speed runs down. Furthermore, although, the system operates in a stable region when the thermal effects are

neglected, however, instability will cause trouble in the same speed due to rising temperatures.

DECLARATION OF ETHICAL STANDARDS

The author(s) of this article declare that the materials and methods used in this study do not require ethical committee permission and/or legal-special permission.

AUTHORS' CONTRIBUTIONS

Abdurrahim DAL: Performed the experiments and analyse the results, and wrote the manuscript.

CONFLICT OF INTEREST

There is no conflict of interest in this study.

REFERENCES

- [1] Zhang Y., Wang W., Wei D., Wang G., Xu J., Liu K., "Coupling analysis of tribological and dynamical behavior for a thermal turbulent fluid lubricated floating ring bearing-rotor system at ultra-high speeds", *Tribology International*, 165: 107325, (2022).
- [2] Shi J., Zhao B., He T., Tu L., Lu X., Xu H., "Tribology and dynamic characteristics of textured journal-thrust coupled bearing considering thermal and pressure coupled effects", *Tribology International*, 180: 108292, (2023).
- [3] Xu B, Guo H, Wu X, He Y, Wang X, Bai J., "Static and dynamic characteristics and stability analysis of high-speed water-lubricated hydrodynamic journal bearings", *Proceedings of the Institution of Mechanical Engineers, Part J: Journal of Engineering Tribology*, 236(4): 701-720, (2022).
- [4] Sun X., Sepahvand K.K., Marburg S., "Stability Analysis of Rotor-Bearing Systems under the influence of misalignment and parameter uncertainty", *Applied Sciences*, 11: 7918, (2021).
- [5] Li Y., Liang F., Zhou Y., Ding S., Du F., Zhou M., Bi J., Cai Y., "Numerical and experimental investigation on thermohydrodynamic performance of turbocharger rotor-bearing system", *Applied Thermal Engineering*, 121: 27-38, (2017).
- [6] Tammineni N.M., Mutra R.R., "A review on recent advancements in an automotive turbocharger rotor system supported on the ball bearings, oil film and oil-free bearings", *Journal of Brazilian Society of Mechanical Science and Engineering*. 45: 481, (2023).
- [7] Feng H., Jiang S., Ji A., "Investigations of the static and dynamic characteristics of water-lubricated hydrodynamic journal bearing considering turbulent, thermohydrodynamic and misaligned effects", *Tribology International*, 130: 245-260, (2019).
- [8] Garg H.C., Kumar V., Sharda H.B., "Performance of slot-entry hybrid journal bearings considering combined influences of thermal effects and non-Newtonian behavior of lubricant", *Tribology International*, 43(8): 1518-1531, (2010).
- [9] Dowson D., Hudson J.D., Hunter B., March C.N., "An experimental investigation of the thermal equilibrium of steadily loaded journal bearings", *Proceedings of Institution of Mechanical Engineering Conference Proceedings*, 181: 70-80, (1966).
- [10] Maneshian B., Nassab S.A.G., "Thermohydrodynamic analysis of turbulent flow in journal bearings running under different steady conditions", *Proceedings of the Institution of Mechanical Engineers, Part J: Journal of Engineering Tribology*. 223(8): 1115-1127, (2009).
- [11] Suganami T., Szeri A.Z., "A thermohydrodynamic analysis of journal bearings", *Trans. ASME, Journal of Lubrication Technology*, 101: 7-21, (1979).
- [12] Pai R.S., Pai R., "Stability of four-axial and six-axial grooved water-lubricated journal bearings under dynamic load", *Proceedings of the Institution of Mechanical Engineers, Part J: Journal of Engineering Tribology*. 222(5): 683-691, (2008).
- [13] Shyu S., Fuli L., Yeau-Ren J., Wei-Ren L., Sheng-Jii H., "THD effects of static performance characteristics of infinitely wide turbulent journal bearings", *Tribology Transactions*, 53(6): 948-956, (2010).
- [14] Shyu S.H., Lee W.R., Hsieh S.J., Liang S.M., "Static performance characteristics of finite-width turbulent journal bearings with THD effect", *Tribology Transactions*, 55(3): 302-312, (2012).
- [15] Tala-Ighil N., Fillon M., "A numerical investigation of both thermal and texturing surface effects on the journal bearings static characteristics", *Tribology International*, 90: 228-239, (2015).
- [16] Li B., Sun J., Zhu S., Fu Y., Zhao X., Wang H., Qing T., Ren Y., Li Y., Zhu G., "Thermohydrodynamic lubrication analysis of misaligned journal bearing considering the axial movement of journal", *Tribology International*, 135: 397-407, (2019).
- [17] Zhu S., Sun J., Li B., Zhu G., "Thermal turbulent lubrication analysis of rough surface journal bearing with journal misalignment", *Tribology International*, 144: 106109, (2020).
- [18] Xu B, Guo H, Wu X., He Y, Wang X, Bai J., "Static and dynamic characteristics and stability analysis of high-speed water-lubricated hydrodynamic journal bearings", *Proceedings of the Institution of Mechanical Engineers, Part J: Journal of Engineering Tribology*. 236(4): 701-720, (2022).
- [19] Klit P., Lund J.W., "Calculation of the dynamic coefficients of a journal bearing, using a variational approach", *ASME. Journal of Tribology*, 108(3): 421-424, (1986).
- [20] Sawicki J.T., Rao T.V.V.L.N., "Nonlinear prediction of rotordynamic coefficients for a hydrodynamic journal bearing", *Tribology Transactions*, 44(3): 367-374, (2001).
- [21] Majumdar B.C., Pai R., Hargreaves D.J., "Analysis of water-lubricated journal bearings with multiple axial grooves", *Proceedings of the Institution of Mechanical Engineers, Part J: Journal of Engineering Tribology*. 218(2): 135-146, (2004).
- [22] Pai R., Rao D.S., Shenoy B.S., Pai R.S., "Stability characteristics of a Tri-taper journal bearing: A linearized perturbation approach", *Journal of Materials Research and Technology*, 1(2): 84-90, (2012).
- [23] Nagaraju Y., Joy M.L., Prabhakaran N.K., "Thermohydrodynamic analysis of a two-lobe journal

- bearing”, *International Journal of Mechanical Science*, 36(3): 209–217, (1994).
- [24] Xu G., Zhou J., Geng H., Lu M., Yang L., Yu L., “Research on the static and dynamic characteristics of misaligned journal bearing considering the turbulent and thermohydrodynamic effects”, *ASME. J. Tribol.*, 137 (2): 024504, (2015).
- [25] Shi J., Zhao B., He T., Tu L., Lu X., Xu H., “Tribology and dynamic characteristics of textured journal-thrust coupled bearing considering thermal and pressure coupled effects”, *Tribology International*, 180: 108292, (2023).
- [26] Dal A., Şahin M., Kilic M., “A thermohydrodynamic performance analysis of a fluid film bearing considering with geometrical parameters”, *Journal of Thermal Engineering*, 9(6): 1604-1617, (2023).
- [27] Dal A., Sahin M., Kilic, M., “Effects of geometrical parameters on thermohydrodynamic performance of a bearing operating with nanoparticle additive oil”, *Industrial Lubrication and Tribology*, 75(2): 255-262, (2023).
- [28] Ferron J., Frene J., Boncompain R., “A study of the thermohydrodynamic performance of a plain journal bearing comparison between theory and experiments”, *ASME. J. of Lubrication Tech.*, 105(3): 422–428, (1983).
- [29] Dal, A., “İki Serbestlik Dereceli Rotor-Hidrokinamik Yatak Sisteminin Kararlılığının Termal Etki Altında İncelenmesi”, *International Journal of Engineering Research and Development*, 16(1): 304-319, (2024).
- [30] Saruhan, H., Kam, M., and Kara, F. “Dynamic Behavior Analysis of Rotor Supported by Damped Rolling Element Bearing Housing”, *Journal Of Polytechnic*, 20(1): 159-164, (2017).
- [31] Şimşek, M., Salman, Nteziyaremye, Ö., Kaleli, H, Tunay, R., F., Durak, E., “Experimental Analysis of Effect to Friction of Commercial Oil Additive Used in Automobiles”. *Journal Of Polytechnic*, 1–1, (2024). <https://doi.org/10.2339/politeknik.1204731>.
- [32] Gürkan, D., Okur, M., ve Korkut, İ. “Döngüsel Kompresörlerde Teknolojik Gelişmeler”, *Journal Of Polytechnic*, 26(1): 425-436, (2023).